Research Article Vol. 56, No. 16 / June 1 2017 / Applied Optics 4695

applied optics

Performance improvement of coherent free-space optical communication with quadrature phase-shift keying modulation using digital phase estimation

Xueliang Li,[1,2,*] Tianwen Geng,[1] Shuang Ma,[1] Yatian Li,[1,2] Shijie Gao,[1] and Zhiyong Wu[1]

[1]Changchun Institute of Optics, Fine Mechanics and Physics, Chinese Academy of Sciences, Dongnanhu Road 3888, Changchun 130033, China
[2]University of Chinese Academy of Sciences, Beijing 100049, China
*Corresponding author: lixueliang0202@163.com

Received 22 February 2017; revised 19 April 2017; accepted 8 May 2017; posted 9 May 2017 (Doc. ID 287296); published 30 May 2017

The performance of coherent free-space optical (CFSO) communication with phase modulation is limited by both phase fluctuations and intensity scintillations induced by atmospheric turbulence. To improve the system performance, one effective way is to use digital phase estimation. In this paper, a CFSO communication system with quadrature phase-shift keying modulation is studied. With consideration of the effects of log-normal amplitude fluctuations and Gauss phase fluctuations, a two-stage *M*th power carrier phase estimation (CPE) scheme is proposed. The simulation results show that the phase noise can be suppressed greatly by this scheme, and the system symbol error rate performance with the two-stage *M*th power CPE can be three orders lower than that of the single-stage *M*th power CPE. Therefore, the two-stage CPE we proposed can contribute to the performance improvements of the CFSO communication system and has determinate guidance sense to its actual application.

OCIS codes: (060.4510) Optical communications; (060.1660) Coherent communications; (060.2605) Free-space optical communication; (060.5060) Phase modulation; (010.1330) Atmospheric turbulence.

https://doi.org/10.1364/AO.56.004695

1. INTRODUCTION

Free-space coherent optical communication is continuously being studied because due to its higher sensitivity than traditional non-coherent optical communication, it has great potential to be used in free-space communication links with a long range and high data rate property [1–3]. Compared to the traditional direct detection (DD) system, even though the coherent detection system is more complicated, it presents the following advantages [4–6]. First, it has higher sensitivity and spectrum efficiency than DD systems, and a great sensitivity can be achieved when homodyne detection is used. Second, the opto-electronic conversion process is linear; the whole optical signal information can be post processed in the electrical domain so that this scheme is applicable to multilevel modulation formats such as *M*-array phase shift keying (PSK) (MPSK) and quadrature amplitude modulation (QAM). However, one of the major challenges in coherent detection is to overcome the carrier phase noise when using a local oscillator (LO) to beat with the received signals to retrieve modulated phase information. In the free-space coherent optical communication system, the phase noise is mainly induced by wavefront distortion resulting from atmospheric turbulence, the linewidth of the lasers, frequency and initial phase offset, and additive noise in the coherent receiver [7]. Therefore, it is the key for the system design to suppress phase noise and synchronize the carrier phase.

With the availability of high-speed digital signal processing (DSP), digital phase estimation provides an alternative for recovering the carrier phase. There are two parameters that need to be considered in the carrier phase estimation (CPE) algorithms. One is linewidth tolerance and the other is hardware complexity. The former determines the robustness of the CPE algorithms and the latter directly affects their applications in practical real-time systems [8]. Feed-forward algorithms are widely used in the CPEs since the feedback algorithms have high hardware requirements [9,10]. Among those feed-forward algorithms, the Viterbi and Viterbi phase estimation (VVPE) [11] algorithm and the blind phase search (BPS) algorithm are two classic CPE algorithms [12]. The VVPE has very low computational complexity but poor estimation accuracy. On the contrary, the BPS has very high estimation accuracy if the number of test phase angles is enough, but has very high computational complexity. To solve this contradiction, multistage CPE algorithms have been proposed in [13,14]. Two-stage CPE is often accepted, in which the first stage is designed for coarse CPE and the second stage for fine CPE.

The multistage CPE algorithms reduce the complexity compared with the single-stage BPS algorithm, but still have higher complexity than the VVPE algorithm. For high-speed optical transmission systems, it is critical for practical realization of real-time coherent optical systems to reduce the complexity of CPE algorithms as far as possible with a tolerable deterioration of performance. The VVPE is the most commonly used technique, which removes the encoded phase data by the Mth power function. It has been demonstrated to be effective in optical fiber communication systems and coherent free-space optical (CFSO) communication systems [15,16]. However, two-stage CPE has not been applied in CFSO systems. It is an effective way to suppress the phase noise induced by atmospheric turbulence. So, we plan to introduce it into the CFSO system, and we propose a two-stage Mth power CPE to balance the computational complexity and estimation accuracy.

This paper describes the coherent optical communication system under the condition of weak atmospheric turbulence with a quadrature phase-shift keying (QPSK) modulation regime at the rate of 20 Gbps. In order to overcome the phase fluctuation induced by atmosphere more effectively, we propose a two-stage Mth power CPE. The first stage is designed for the coarse estimation and the second stage is designed for the fine estimation. The simulation results show that the proposed two-stage CPE scheme can improve the symbol error rate (SER) performance of the CFSO system significantly.

The remainder of the paper is organized as follows. In Section 2, the system structure and channel statistics are introduced. The log-normal distributed channel statistics are described. Receiver theory is introduced in Section 3. The phase estimation algorithm is analyzed in Section 4. In Section 5, the simulation parameters are analyzed and listed, and a number of numerical results are presented to show the advantages of using the phase estimation algorithm to improve system performance. Finally, some concluding remarks are provided in Section 6.

2. CHANNEL STATISTICS AND SYSTEM STRUCTURE

A. Channel Statistics

In free-space optical (FSO) systems, one of the remaining impediments is atmospheric scintillation, which, resulting from the index of refraction fluctuations, can cause fading in FSO systems. The statistics of the strength of scintillation events are generally regarded as following the log-normal distribution. Often the Rytov variance, σ_R^2, is used to describe the irradiance fluctuations due to scintillation for the case of weak fluctuations when using the Kolmogorov spectrum [17],

$$\sigma_R^2 = 1.23 C_n^2 k^{7/6} L^{11/6}, \tag{1}$$

where, C_n^2 is the atmospheric structure constant which is a measure of the strength of the scintillation. For a FSO system near the ground, it varyies from 10E – 17 $m^{-2/3}$ to 10E – 13 $m^{-2/3}$ according to the atmospheric turbulence conditions. $k = 2\pi/\lambda$ is the wave number and L is the link length. $\sigma_R^2 < 1$, $\sigma_R^2 \approx 1$, and $\sigma_R^2 > 1$ stand for the weak, moderate, and strong intensity scintillation, respectively.

The most common channel model for the description of atmospheric turbulence is log-normal distribution. The distribution of log-amplitude fluctuation is Gaussian distribution, so that the probability distribution function (PDF) of the received irradiance I is given as

$$p_I(I) = \frac{1}{I\sigma\sqrt{2\pi}} \exp\left\{-\frac{1}{2\sigma^2}\left[\ln\left(\frac{I}{I_0}\right) + 0.5\sigma^2\right]^2\right\}, \tag{2}$$

where I_0 is known as irradiance when there is no turbulence and σ^2 is the normalized variance of irradiance, also called the scintillation index. Under weak fluctuation conditions, the normalized variance of irradiance is approximately equal to the Rytov variance.

B. System Structure

The structure of the coherent optical system model is described in Fig. 1. In the transmitter, a Mach–Zehnder modulator (MZM) is used to modulate the laser. The in-phase and the quadrature branches of the MZM are driven by two electrical pseudo-random binary sequences (PRBS). The modulated optical signal is amplified by erbium-doped fiber amplifier (EDFA) and transmitted over the transmitter antenna.

In the coherent receiver, the received optical signal, after passing through the free-space link, is amplified by the EDFA, and a homodyne inphase-quadrature receiver (IQ-receiver) is used for signal detection. The state of the polarizations (SOP) of the local oscillator (LO) and received signal are assumed to be the same by using the polarization controller (PC). The received signal beats with the local oscillator in a $2 \times 490°$ hybrid, and the output signals are detected by two balanced photodetectors (BD). The resulting electrical in-phase and quadrature signals are then further processed by high-speed digital signal processing for carrier synchronization via digital phase estimation.

3. RECEIVER THEORY

Coherent detection involves an incoming signal beating with a LO beam. To evaluate the impact of turbulence, the combined effects of log-amplitude fluctuations (scintillation) and Gaussian phase fluctuations (aberrations) should be considered. Consequently, the received signal field and LO field in the receiver plane can be expressed as

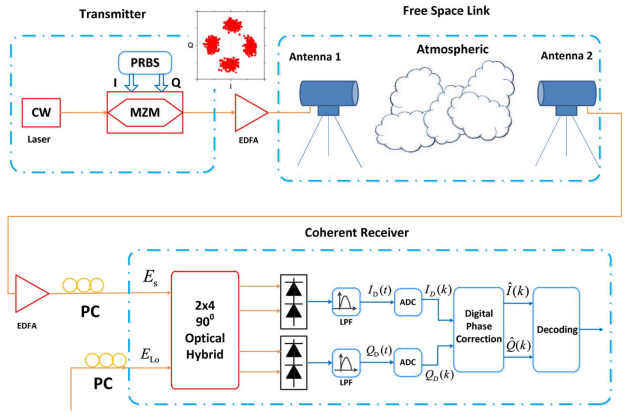

Fig. 1. Schematic of CFSO system. CW, continuous wave laser; MZM, Mach–Zehnder modulator; EDFA, erbium-doped fiber amplifier; PC, polarization controller.

$$E_r(r,t) = E_s \exp[(\chi(r) + j\phi(r))]\exp[j(\omega_s t + \theta_s(t) + \theta_{ns}(t))]$$
$$E_{\mathrm{LO}}(t) = E_l \exp[j(\omega_l t + \theta_{nl}(t))], \quad (3)$$

where E_S and E_{LO} represent the amplitude of the signal laser and local oscillator, ω_s and ω_l are the angular frequencies, $\exp(\chi(\mathbf{r}))$ and $\exp(j\phi(\mathbf{r}))$ represent the turbulence-induced log-normal amplitude fluctuations and Gaussian phase fluctuations, respectively [18]. The log-amplitude variance can be represented by scintillation index σ_I^2 in weak fluctuation theory as

$$\sigma_\chi^2 = \frac{1}{4}(1+\sigma_I^2)\sigma_I^2 = \sigma_R^2 = 1.23C_n^2k^{7/6}L^{11/6}. \quad (4)$$

We think that phase $\phi(\mathbf{r})$ obeys zero-mean Gaussian statistics. Supposing a Kolmogorov spectrum of turbulence, the classical statistics of phase variance σ_ϕ^2 were extended to consider modal compensation of atmospheric phase distortion. In such modal compensation, the residual phase σ_ϕ^2 is usually denoted by Zernike polynomials for their simple analytical expressions and their correspondence to classical aberrations [19,20]. It is known that the residual phase variance after modal compensation of J Zernike terms is given by

$$\sigma_\phi^2 = C_J\left(\frac{D}{r_0}\right)^{5/3}, \quad (5)$$

where D is the aperture diameter and r_0 is the Fried parameter, which describes the spatial correlation of phase fluctuations in the receiver plane. For plane waves and Kolmogorov turbulence, r_0 can be expressed in terms of the wavenumber k, the refractive index structure constant C_n^2, and the propagation distance L as $r_0 = 1.68(C_n^2Lk^2)^{-3/5}$ [21]. The coefficient $C_J = 1.0299$ in the phase variance σ_ϕ^2 assumes that no terms are corrected by a receiver employing active modal compensation [22]. In Eq. (5), the receiver aperture diameter D is normalized by the wavefront coherence diameter r_0, which describes the spatial correlation of phase fluctuations in the receiver plane. In this paper we consider the situation that the aperture diameter is much smaller than the coherence diameter, $D \ll r_0$, so that the beam in the receiver plane is spatially coherent at a single instant in time. So the received signal field can be expressed as

$$E_r(t) = E_s \exp(\chi(t) + j\phi(t))\exp[j(\omega_s - \omega_l)t + \theta_s(t) + \theta_{ns}(t))], \quad (6)$$

where $\theta_s(t)$ is the modulated phase with a value of $0, \pi/2, \pi, -\pi/2$, $\theta_{ns}(t)$ is the carrier phase in reference to the LO phase, and we assume that the phase difference $\theta_{ns}(t+T) - \theta_{ns}(t)$ in a symbol interval T follows a Gaussian distribution with a variance $\sigma_p^2 = 4\pi\Delta f T$, where Δf denotes the combined linewidth of the transmitter and LO [23].

In a homodyne coherent receiver ($\omega_s = \omega_l$), the received signal is combined with the light of a LO in a $2 \times 490°$ optical hybrid, and yield the output fields

$$\begin{bmatrix} E_1 \\ E_2 \\ E_3 \\ E_4 \end{bmatrix} = \frac{1}{2}\begin{bmatrix} 1 & 1 \\ 1 & j \\ 1 & -1 \\ 1 & -j \end{bmatrix} \cdot \begin{bmatrix} E_s(t) \\ E_{\mathrm{LO}} \end{bmatrix} = \begin{bmatrix} E_s(t)/2 + E_{\mathrm{LO}}/2 \\ E_s(t)/2 + jE_{\mathrm{LO}}/2 \\ E_s(t)/2 - E_{\mathrm{LO}}/2 \\ E_s(t)/2 - jE_{\mathrm{LO}}/2 \end{bmatrix}. \quad (7)$$

Detecting E_1 and E_3 with the upper, and E_2 and E_4 with the lower BD, then the resulting photocurrents in-phase and quadrature signals can be calculated by

$$I_D(t) = RE_lE_s(t)\cos(\theta_s(t) + \theta_n(t)) + n_I(t)$$
$$Q_D(t) = RE_lE_s(t)\sin(\theta_s(t) + \theta_n(t)) + n_Q(t), \quad (8)$$

where R represents the responsivity of the photodiode, and $E_s(t)$ is the received signal amplitude including log-normal amplitude fluctuation. In this paper we consider $\theta_n(t)$ as the total phase error between the carrier and the local oscillator, which is the integrative effects of atmospheric turbulence and laser linewidth. The shot noise and thermal noise are both taken into account in the system and can be modeled as additive white Gaussian noise (AWGN). $n_I(t)$ and $n_Q(t)$ represent the cumulative additive white Gaussian noise signal consisting of thermal, shot, and amplified spontaneous emission (ASE) noise.

After being filtered, the signal $I_D(t)$ and $Q_D(t)$ given by Eq. (8) are simultaneously sampled once every symbol period T with analog-to-digital converters (ADCs). We obtain the complex samples of the received complex envelope

$$E(k) = I_D(k) + jQ_D(k). \quad (9)$$

Then the sampled signal $I_D(k)$ and $Q_D(k)$ are processed with the phase estimation algorithm to get the estimation of total phase error θ_e for each symbol. Having the information of the total phase error we are able to rotate the actual constellation point by the negative total phase error. The details are described in Section 4.

4. PHASE ESTIMATION ALGORITHM

A. Single-Stage Phase Estimation Algorithm

In this paper, the Mth power scheme of feed-forward phase estimation is used, and the structure of this algorithm is shown in Fig. 2. For QPSK modulation, $M = 4$. The modulated data $\theta_s(t)(= 0, \pi/2, \pi, -\pi/2)$ is removed by the fourth power function $(\bullet)^4$ since $4\theta_s(t) = 4\pi * m$ (m is integer), regardless of $\theta_s(t)$'s value. So $E^4(k) \propto \exp[j4\theta_n]$ and the operation $1/4 * \arg(\bullet)$ seem to get complete information about the phase noise $\theta_n(t)$ at each sample. The optical carrier phase $\theta_s(t)$ varies much more slowly than the phase modulation, whose symbol rate is equal to 10G symbol/s in our experiments. Therefore, by averaging the carrier phase over many symbol intervals, it is possible to obtain an accurate phase estimate. The complex amplitude $E^4(k)$ is summed, so that the phase is averaged over N neighbor symbols,.then the phase of the resulting complex amplitude is divided by 4, leading to a phase estimate, $\theta_e \in (-\pi/4, \pi/4)$, which is common to all the samples in the block and is given by [23]

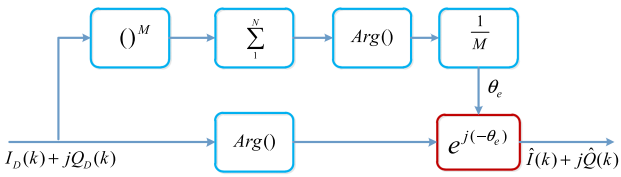

Fig. 2. Structure of Mth power phase estimation algorithm.

$$\theta_e = \frac{1}{4}\mathrm{Arg}\left\{\sum_{n=1}^{N}[E(k)]^4\right\}. \quad (10)$$

It is important to note that differential encoding/decoding has been applied to solve the phase ambiguity problem, even if we do not employ differential detection. For synchronous coherent detection, differential precoding can solve the phase ambiguity, so that the unwrap function is unnecessary. The signals $I_D(k)$ and $Q_D(k)$ are processed with the phase estimation algorithm to get the estimation of phase error θ_e for each symbol. Then we can get the estimation of the signals as

$$\hat{I}(k) + j\hat{Q}(k) = [I_D(k) + jQ_D(k)] \cdot e^{j(-\theta_e)}. \quad (11)$$

There is an evident trade-off here: in principle, a short average length N enables fast carrier phase tracking but is limited by the speed of DSP, and a long average length N enables large noise tolerance but the phase estimate is then common on more samples, thus reducing the phase estimate accuracy on each sample. The optimum length is given by a balance between the two factors [24]. An optimal average length is determined according to the system condition in this paper. As we can see in Fig. 3, the SER performance degrades with the increase of linewidth of the signal laser and LO for the same average length. The increase of linewidth results in the increase of phase variance $\sigma_p^2 = 4\pi\Delta f T$, so the SER performance degrades. In the case of the same linewidth, note that with the decrease of N the SER reduces significantly. It is obvious that the noise tolerance degrades as the N increases and a distinct decrease of SER appears when $N \geq 10$. Because a long average length N means that a large number of samples will share the same estimated phase, the phase estimate accuracy on each sample is reduced. As depicted in Fig. 3, $N = 10$ is a limit average length for single-stage phase estimation algorithm.

For the consideration of various factors such as noise tolerance, carrier phase tracking, and the complexity of algorithm, we think that $N = 10$ is the optimal average length for this system, and similar conclusions can be found in [23,25].

B. Two-Stage Phase Estimation Algorithm

In order to improve the estimation accuracy, in this paper, we also designed a second-stage CPE. The corrected signal based on the Mth power phase estimate method above will be passed into another Mth power phase estimation stage to further refine the phase estimation, as shown in Fig. 4. This is a new scheme we first proposed in this paper. In this new scheme, the first stage is designed for the coarse estimation and the second stage is designed for the fine estimation, which has both advantages of good noise tolerance and fast carrier phase tracking. The average length N_1 in the first stage Mth power CPE is set to be small to guarantee the fast carrier phase tracking and the large N_2 in the second stage Mth power CPE to ensure the good noise tolerance. There is another trade-off here: how to select the optical lengths for N_1 and N_2. Figure 5 shows the simulated SER performance versus the linewidth with different combinations of N_1 and N_2. For comparison, $N = 10$ for the single-stage CPE scheme is also shown in Fig. 5. It can be seen that the SER performance of the two-stage scheme outperforms the single-stage scheme and $N_1 = 3, N_2 = 7$ is the best combination for the two-stage scheme. As explained above, the first stage is designed for the coarse estimation and the second stage is designed for the fine estimation. The average length N_1 in the first stage is set to be 3 to guarantee the fast carrier phase tracking, because a small average length leads to low complexity and quick operation speed. The second stage average length N_2 is set to 7 to ensure the good noise tolerance, because a large average length leads to noise suppression ability. Therefore, this combination of N_1

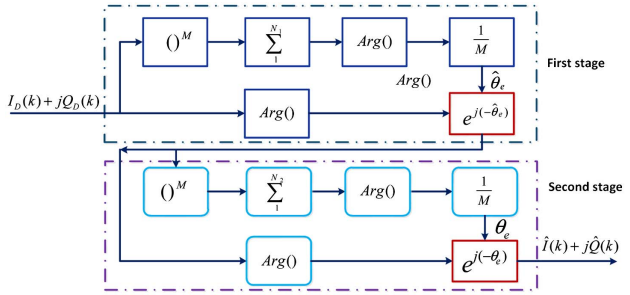

Fig. 4. Block diagram of the proposed two-stage CPE.

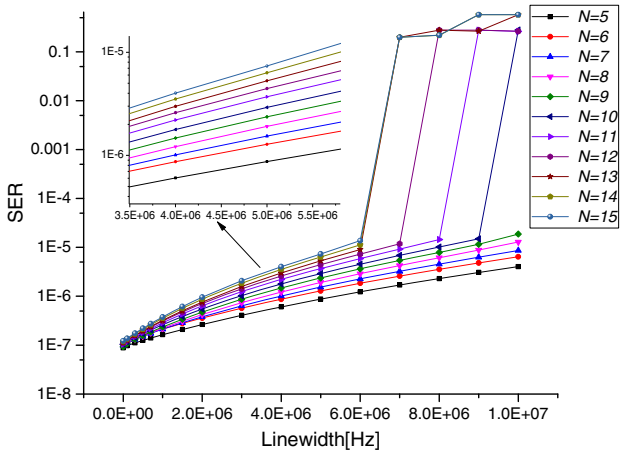

Fig. 3. SER performance versus linewidth with different N for single-stage CPE.

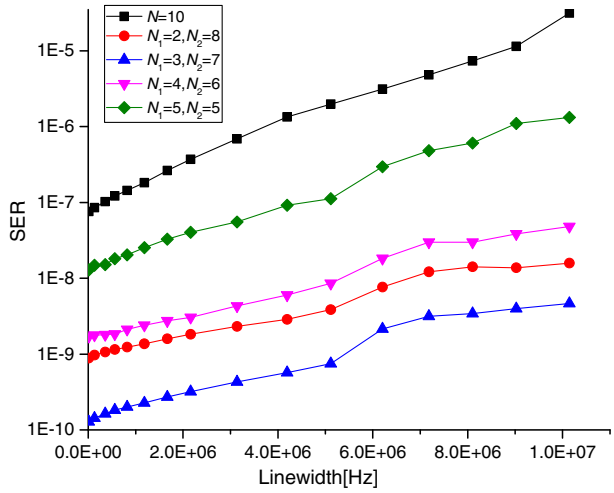

Fig. 5. SER performance versus linewidth with different combinations of N_1 and N_2. $N = 10$ stands for single-stage CPE.

and N_2 has both advantages of good noise tolerance and fast carrier phase tracking. However, it should be noted that the optimal combination of N_1 and N_2 is not fixed and it varies based on turbulence conditions and system configurations. In a word, no matter which combination of N_1 and N_2, the SER performance of the two-stage CPE outperforms the single-stage scheme and can do so by three orders lower when $N_1 = 3$, $N_2 = 7$.

5. NUMERICAL RESULTS AND DISCUSSION

The simulations were performed with the commercial software tools Virtual Photonics Inc. (VPI) transmission maker and MATLAB to prove the proposed phase estimation algorithm. With VPI, the QPSK transmitter is configured, composed of PRBS generator, the electrical level generator, and the modulator driver, as well as the conventional optical IQ-modulator, which has a pair of single drive MZMs (IQ_SD). In the transmitter, the wavelength of the laser is 1550 nm and the linewidth of the signal laser and the LO is 100 kHz. The data rate is 20 Gbps (corresponding to 10 Gsymbol/s), and the length of the PRBS sequence is $2^7 - 1$. The modulated optical signal is launched into the EDFA, which can amplify the output power to 10 dBm. Then the laser beams are transmitted in free space and detected by positive-intrinsic-negative (PIN) BD. The optical turbulence parameters are presented in Table 1. As one can see from Table 1, the laser beam will suffer from a very weak scintillation effect and the aperture diameter is much smaller than the coherence diameter, $D \ll r_0$, so the wavefront is coherent within the receiver aperture at a single instant in time. The received optical signal, after passing through the free-space link, is amplified by the EDFA. The received optical power is −20 dBm. Free-space power attenuation is about 30 dB. The frequency offset of the signal laser and the LO varies (0–200 MHz). The shot noise (SN) is included, and the thermal noise (TN) is 10E − 12. Analog-to-digital conversion (ADC) of the two quadratures is performed at the symbolrate (e.g., 10 Gsample/s/quadrature for a 20 Gbps QPSK signal). Each pair of samples (the in-phase and quadrature samples) is combined into a single complex sample. The samples of the received signals of the I-arm and the Q-arm are processed by the phase estimation algorithm implemented in MATLAB. The symbol error rate (SER) and error vector magnitude (EVM) are estimated by VPI software according to the parameter settings.

Figure 6 shows that the improvement of the IQ plot (constellation), including phase noise, with the phase estimation method. The linewidth is set as 100 KHz. We can see that

Table 1. Parameters Used in the Numerical Simulation

Parameter	Value
Wavelength	1550 nm
Aperture diameter D	5 cm
C_n^2	1.5E − 15 $m^{-2/3}$
Atmospheric coherent diameter r_0	24.5 cm
Transmission distance L	1000 m
Rytov variance σ_R	0.17
Phase variance σ_ϕ	0.07 rad

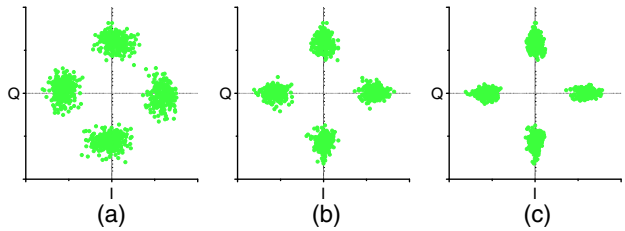

Fig. 6. Normalized constellation diagram of QPSK signal with laser linewidth 100 KHz for the transmitter and the local oscillator (a) before CPE, (b) after single-stage CPE, and (c) after two-stage CPE.

the constellation with phase noise (a) is improved obviously after single-stage phase estimation (b) and further improved after two-stage phase estimation (c). The constellations show random distribution around their expected position due to phase noise resulting from linewidth and turbulence, and they are now in a relatively correct position after CPE, as we expected Similarly, Fig. 7 shows the improvement of the constellation with CPE, including frequency offset of 20 MHz between the signal laser and LO. As we can see from Fig. 7, the constellations show random distribution and form a "ring" due to phase noise and amplitude noise, and they are now in a relatively correct position after phase correction. The corrected symbols show radial noise distributions due to the correction with the total phase error, except for the case with additional correction of the amplitude.

As one can see from Fig. 8, based on the method described above, the SER performance of the system is plotted as a function of linewidth and $N = 10$ for the single-stage CPE, $N_1 = 3$, $N_2 = 7$ for the two-stage. Note that the system performance is degraded seriously due to turbulence even when the linewidth is 20 KHz, and the phase estimation algorithm can greatly improve the system performance under the same conditions. When the linewidth of the signal and the local oscillator is increased to 10 MHz, the improvement can also be observed and a SER performance of 10^{-8} can be obtained. Also, the SER of the two-stage Mth power CPE can be three orders lower than that of the single-stage scheme.

Figure 9 illustrates the SER performance as a function of linewidth with different frequency offsets. The phase drift in the receiver caused by the frequency difference between the transmitter and the local oscillator can be compensated for with the CPE. The constant frequency offset can be compensated for by differential precoding and differential decoding. It is evident

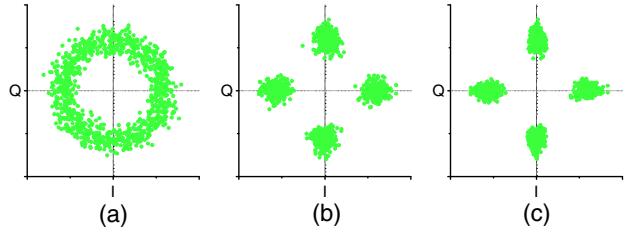

Fig. 7. Normalized constellation diagram of QPSK signal with laser linewidth 100 KHz and frequency offset 20 MHz for the transmitter and the local oscillator(a) before CPE, (b) after single-stage CPE, and (c) after two-stage CPE.

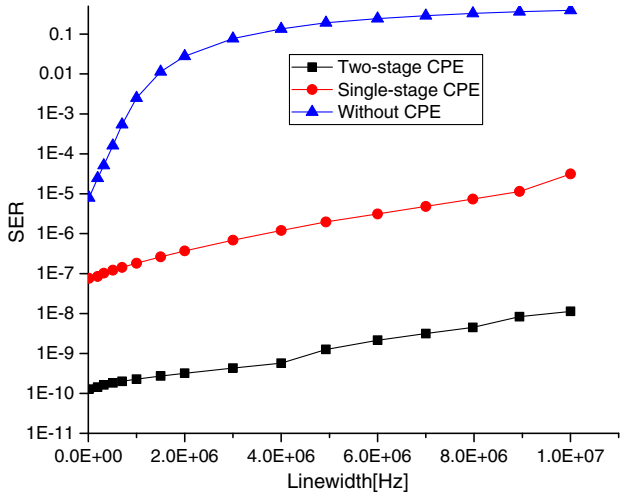

Fig. 8. SER versus linewidth for the two-stage CPE, single-stage CPE, and without CPE.

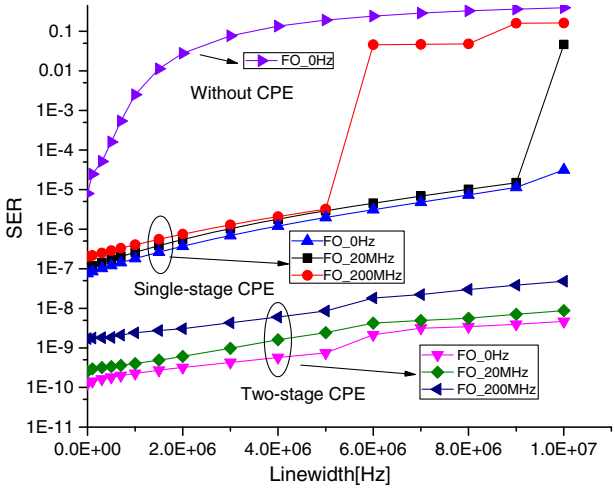

Fig. 9. SER versus linewidth with frequency offset of 0 Hz, 20 MHz, and 200 MHz for the two-stage CPE, single-stage CPE, and without CPE.

that the two-stage scheme outperforms the single-stage. When the frequency offset is increased to 200 MHz, the improvement can also be observed for the two-stage CPE. However, it degrades seriously for the single-stage when the linewidth $\geq$5 MHz; this is due to the fact that the single-stage CPE is not able to track the cycle-slips occurring at higher values of linewidth and frequency offset. On the contrary, it degrades seriously when the linewidth $\geq$9 MHz if frequency offset is 20 MHz.

In order to verify the ability for compensation for the phase noise induced by atmospheric turbulence of the proposed two-stage CPE, different phase variances are set in simulation. $\sigma_\phi = 0.07$, $\sigma_\phi = 0.1$, $\sigma_\phi = 0.13$ stand for different atmospheric conditions, but all stand for weak turbulence. As σ_ϕ increases, the fluctuation of phase becomes severe, so the phase noise induced by atmospheric turbulence becomes terrible.

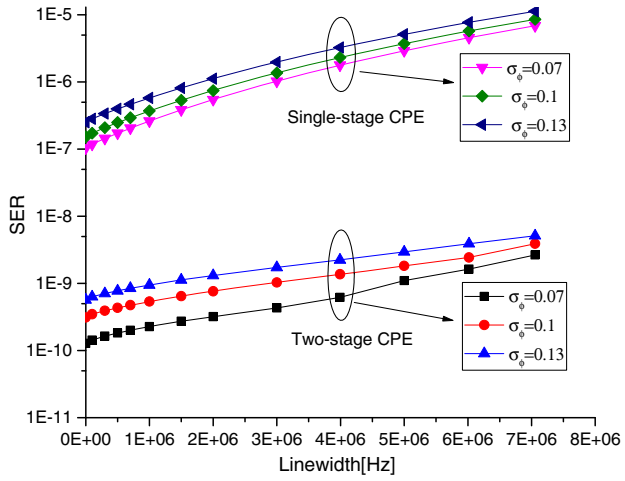

Fig. 10. SER versus linewidth measured with the two-stage CPE and single-stage CPE for $\sigma_\phi = 0.07$, $\sigma_\phi = 0.1$, $\sigma_\phi = 0.13$.

Here, the optical scatter σ_R in atmospheric channel that mainly affects the signal amplitude is not considered, since the Mth power CPE scheme only corrects the phase, but not the amplitude, of the received symbol. As shown in Fig. 10, it is clear that the two-stage scheme outperforms the single-stage scheme significantly at all linewidth values. So, the phase noise induced by atmospheric turbulence can be suppressed effectively by this scheme.

Figure 11 shows another performance measure for advanced modulation formats [26]. It describes the effective distance of the received complex symbol from its ideal position in the constellation diagram. The EVM can be expressed as

$$\mathrm{EVM} = \sqrt{\frac{\sum_{i=1}^{N_s} |\mathrm{IQ} - \mathrm{IQ}tx|^2}{\sum_{i=1}^{N_s} |\mathrm{IQ}tx|^2}}, \tag{12}$$

where IQ is the normalized nth symbol in the stream of measured symbols, IQtx is the ideal normalized constellation point of the nth symbol, and N_s is the number of unique symbols in

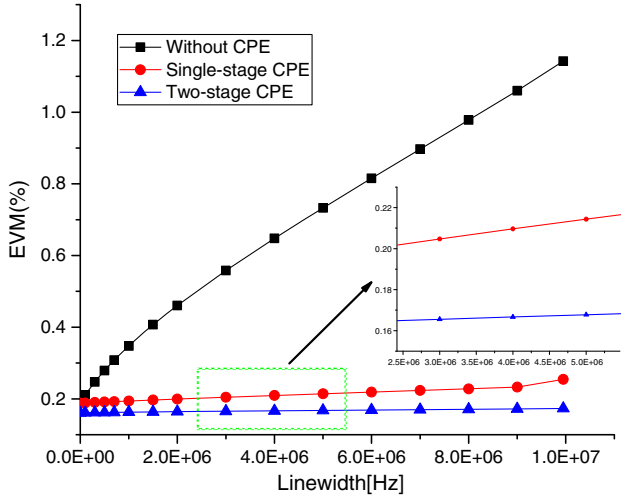

Fig. 11. EVM versus linewidth for the two-stage CPE, single-stage CPE, and without CPE with frequency offset of 20 MHz.

the constellation. Similar to Figs. 8–10, we can see that the EVM performance can be greatly improved with the phase estimation method even though there is frequency offset. From another point of view, our phase estimation scheme is feasible for a CFSO system.

6. CONCLUSIONS

In this paper, we have investigated a CFSO system with QPSK modulation, and the effects of log-normal amplitude fluctuations and Gauss phase fluctuations are considered. A two-stage Mth power CPE scheme is proposed and the system performance improvement due to this scheme is investigated by simulation. The simulation results show that the deterioration induced by weak atmospheric turbulence and other phase noise sources can be compensated for greatly. All the simulation results reveal that it is more powerful than the single-stage CPE scheme. The SER could achieve 10E – 8 at the rate of 20 Gbps and the linewidth tolerance can reach to 10 MHz. Hence, the two-stage CPE scheme we proposed can contribute to the performance improvement of the CFSO system and its practical realization.

It should be noted that only the weak turbulence condition is considered in this paper. Issues like the development of further optimized algorithms that are suitable for moderate and strong atmospheric turbulence are for further study.

Funding. National Natural Science Foundation of China (NSFC) (51605465).

Acknowledgment. We thank the Optical Communication Laboratory of CIOMP for the use of their equipment.

REFERENCES

1. M. Niu, X. Song, J. Cheng, and J. F. Holzman, "Performance analysis of coherent wireless optical communications with atmospheric turbulence," Opt. Express **20**, 6515–6520 (2012).
2. A. Belmonte and J. M. Khan, "Capacity of coherent free-space optical links using atmospheric compensation techniques," Opt. Express. **17**, 2763–2773 (2009).
3. K. Kiasaleh, "Performance of coherent DPSK free-space optical communication systems in K-distributed turbulence," IEEE Trans. Commun. **54**, 604–607 (2006).
4. S. M. Aghajanzadeh and M. Uysal, "Diversity-multiplexing trade-off in coherent free-space optical systems with multiple receivers," J. Opt. Commun. Netw. **2**, 1087–1094 (2010).
5. P. Kumar, "Comparative analysis of BER performance for direct detection and coherent detection FSO communication systems," in *Proceedings of IEEE Conference on Communication Systems and Network Technologies* (IEEE, 2015), pp. 369–374.
6. J. Park and E. Lee, "Performance analysis of coherent free-space optical systems with multiple receivers," IEEE Photon. Technol. Lett. **27**, 1010–1013 (2015).
7. N. Perlot, "Turbulence-induced fading probability in coherent optical communication through the atmosphere," Appl. Opt. **46**, 7218–7226 (2007).
8. J. Han, W. Li, L. Huang, H. Li, Q. Hu, and S. Yu, "Carrier phase estimation based on error function calculation for 16-QAM systems," IEEE Photon. Technol. Lett. **28**, 2561–2564 (2016).
9. E. Ip and J. M. Kahn, "Feedforward carrier recovery for coherent optical communications," J. Lightwave Technol. **23**, 4110–4124 (2005).
10. X. Li, Y. Cao, S. Yu, W. Gu, and Y. Ji, "A simplified feedforward carrier recovery algorithm for coherent optical QAM system," J. Lightwave Technol. **29**, 801–807 (2011).
11. A. J. Viterbi and A. N. Viterbi, "Nonlinear estimation of PSK-modulated carrier phase with application to burst digital transmission," IEEE Trans. Inf. Theory **29**, 543–551 (1983).
12. T. Pfau, S. Hoffmann, and R. Noé, "Hardware-efficient coherent digital receiver concept with feedforward carrier recovery for M-QAM constellations," J. Lightwave Technol. **27**, 989–999 (2009).
13. X. Zhou, "An improved feed-forward carrier recovery algorithm for coherent receivers with M-QAM modulation format," IEEE Photon. Technol. Lett. **22**, 1051–1053 (2010).
14. T. Pfau and R. Noé, "Phase-noise-tolerant two-stage carrier recovery concept for higher order QAM formats," IEEE J. Sel. Top. Quantum Electron. **16**, 1210–1216 (2010).
15. P. Liu, J. Yan, and Z. Zheng, "Analysis of improved performance for a satellite-to-ground coherent optical communication system with DQPSK modulation due to phase estimation," in *Communications and Networking in China* (IEEE, 2010).
16. I. Fatadin and D. Ives, "Differential carrier phase recovery for QPSK optical coherent systems with integrated tunable lasers," Opt. Express **21**, 10166–10171 (2013).
17. L. C. Andrews and R. L. Phillips, *Laser Beam Propagation Through Random Media*, 2nd ed. (SPIE, 2005).
18. M. Li and M. Cvijetic, "Coherent free space optics communications over the maritime atmosphere with use of adaptive optics for beam wavefront correction," Appl. Opt. **54**, 1453–1462 (2015).
19. R. J. Noll, "Zernike polynomials and atmospheric turbulence," J. Opt. Soc. Am. **66**, 207–211 (1976).
20. A. Belmonte and J. M. Khan, "Performance of synchronous optical receivers using atmospheric compensation techniques," Opt. Express **16**, 14151–14162 (2008).
21. D. L. Fried, "Optical heterodyne detection of an atmospherically distorted signal wave front," Proc. IEEE **55**, 57–77 (1967).
22. A. Belmonte and J. M. Khan, "Capacity of coherent free-space optical links using diversity-combining techniques," Opt. Express. **17**, 12601–12611 (2009).
23. D. S. Ly-Gagnon, S.Tsukamoto, K. Katoh, and K. Kikuchi, "Coherent detection of optical quadrature phase-shift keying signals with carrier phase estimation," J. Lightwave Technol. **24**, 12–21 (2006).
24. G. Goldfarb and G. Li, "BER estimation of QPSK homodyne detection with carrier phase estimation using digital signal processing," Opt. Express **14**, 8043–8053 (2006).
25. S. Tsukamoto, K. Katoh, and K. Kikuchi, "Coherent demodulation of optical multilevel phase-shift-keying signals using homodyne detection and digital signal processing," IEEE Photon. Technol. Lett. **18**, 1131–1133 (2006).
26. R. Schmogrow, B. Nebendahl, M. Winter, A. Josten, D. Hillerkuss, S. Koenig, J. Meyer, M. Dreschmann, M. Huebner, C. Koos, J. Becker, W. Freude, and J. Leuthold, "Error vector magnitude as a performance measure for advanced modulation formats," IEEE Photon. Technol. Lett. **24**, 61–63 (2012).